Matter

CellPress

Article

Ultrastrong, highly conductive and capacitive hydrogel electrode for electron-ion transduction

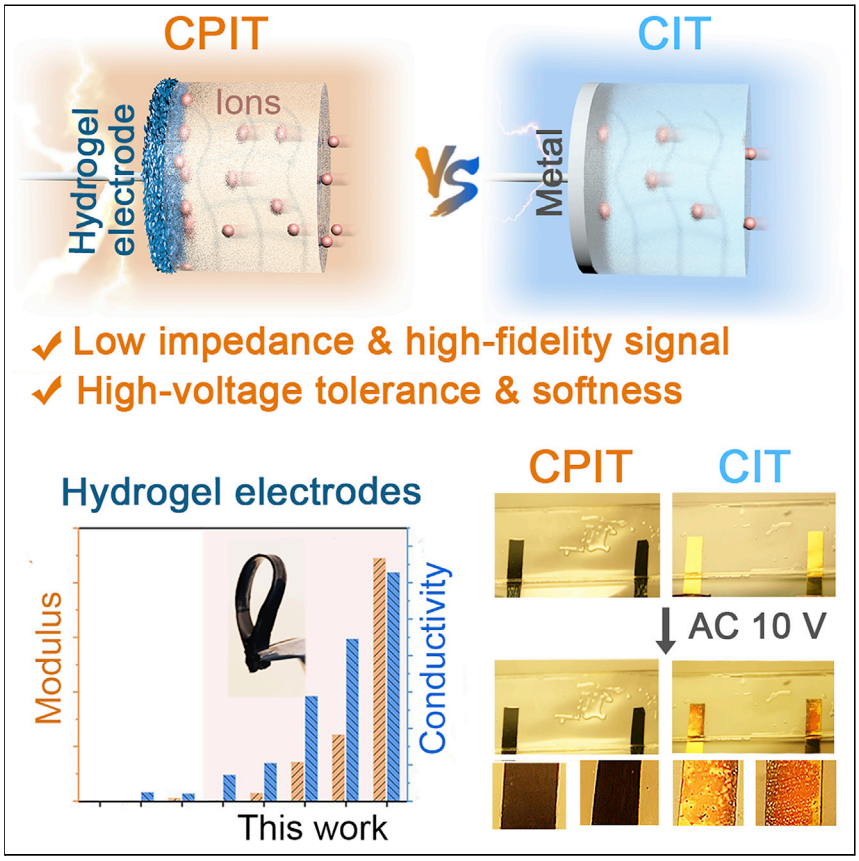

Yao et al. develop conducting polymer hydrogel electrodes by combining pre-gelation with partial densification to resolve the intrinsic conflict among capacitance, conductivity, and mechanical properties in electrode design. With these hydrogel electrodes, signal fidelity, device stability, and voltage tolerance are significantly improved for next-generation biomimetic devices that operate with a hybrid circuit of mobile ions and electrons.

Bowen Yao, Yichen Yan, Qingyu Cui, ..., Xinyuan Zhu, Tzung Hsiai, Ximin He

ximinhe@ucla.edu

Highlights

Hydrogel electrode with excellent electrical and mechanical performance

Ultralow interfacial impedance and high signal fidelity

A new ionotronics model with patternable current density spatial distribution

Heart-pacing electrode with low threshold voltage

Improvement
Enhanced performance with innovative design or material control

Yao et al., Matter 5, 1–18
December 7, 2022
https://doi.org/10.1016/j.matt.2022.09.004

Please cite this article in press as: Yao et al., Ultrastrong, highly conductive and capacitive hydrogel electrode for electron-ion transduction, Matter (2022), https://doi.org/10.1016/j.matt.2022.09.004

Matter

CellPress

Article

Ultrastrong, highly conductive and capacitive hydrogel electrode for electron-ion transduction

Bowen Yao,[1,2,4] Yichen Yan,[1,4] Qingyu Cui,[3] Sidi Duan,[1] Canran Wang,[1] Yingjie Du,[1] Yusen Zhao,[1] Dong Wu,[1] Shuwang Wu,[1,2] Xinyuan Zhu,[2] Tzung Hsiai,[3] and Ximin He[1,5,*]

SUMMARY

Electron-ion transduction is the cornerstone for promoting emerging ionotronic devices, ranging from basic electronic elements to bioelectronics. However, with commonly used metal electrodes, the electron-ion transduction suffers from high impedance, signal distortion, and poor voltage tolerance. Conductive porous electrodes could partially remedy these issues but are accompanied by mechanical weakness. Herein, a general strategy is discovered to ameliorate these issues by introducing a conducting polymer hydrogel electrode of ultrahigh strength and conductivity with a capacitive behavior. These features are derived from a nanoporous conductive matrix that has π-π interactions as both cross-linking sites and electron-transfer pathways and is formed through surface gelation coupled with chemical treatment and controlled densification. This strategy significantly decreases the low-frequency impedance and improves the signal fidelity, without affecting its high-frequency response. Furthermore, excellent biocompatibility and multifunctionality have also been demonstrated, showing the great potential of this strategy for bioelectronic applications and human-machine interfaces.

INTRODUCTION

Whereas living organisms transmit signals via ions,[1] conventional human-made electronic devices rely mostly on electron transport. To bridge the electronic realm and the biological world, two promising technologies—ionotronics and bioelectronics—have emerged, attempting to transduce electronic and ionic signals in both directions. Ionotronic devices are being developed as emerging electronics that are usually constructed using hydrogels and elastomers and function with a hybrid circuit of mobile ions and mobile electrons, while bioelectronics could be considered as one special subset of ionotronics in which the ionic signal originates from living biological tissue. For practical applications, ionotronics are promising to open up numerous unprecedented opportunities in a series of novel stretchable/soft electronics, including energy harvesting,[2–4] ionic transistors,[5] logic circuits,[6] displays,[7] and soft robots,[8,9] while bioelectronics focuses on the convergence of biology and electronics, with the examples of physiological signal sensing for diagnosis[10] and brain-computer interfaces,[11] as well as electrical stimulation for medical therapy.[12,13]

Inert metals have been often employed as the electrodes of current ionotronics and bioelectronics to transduce electronic and ionic signals.[14,15] However, they have several issues, including: (1) a high and unstable impedance across the

PROGRESS AND POTENTIAL

An ideal electrode material for bioelectronics and ionotronics should have a high specific surface area, high electrical conductivity, good mechanical properties, and electrochemical stability. The intrinsic conflicts among capacitance, conductivity, and mechanical properties severely limit the molecular design of electrode materials. The strategy developed in this work, pre-gelation coupled with partial densification, can successfully create high-performance conducting polymer hydrogel electrodes by controlling their porous structure at micro- and nanoscales. By utilizing this hydrogel electrode, the ionic-to-electronic signal conversion and interfacial stability issues of ionotronics were successfully remedied in this work, as an important step toward next-generation electronics connecting the ion and electron realms.

electrode/electrolyte interface, causing a significant loss and distortion of low-frequency signals (<100 Hz), which are highly important in many applications, such as low-grade energy conversion (e.g., low-frequency vibration of <5 Hz),[16] electromechanical transduction (e.g., actuators working at 0.01–100 Hz),[17] and electrophysiological recordings (e.g., neural local field potential, typically <100 Hz),[18] and (2) a high voltage drop across the electrode/electrolyte interface, due to the high impedance at low frequency, inducing undesirable faradic electrochemical reactions. One strategy to remedy this issue is to introduce a faradic process into the electrode (e.g., Ag/AgCl), through which electrochemical reaction current passes. However, this suffers from low interfacial stability, mutable electrode potential, and potential toxicity for long-term implantation.[19,20]

An alternative to employing electrochemical reactions is to modify the inert metal electrodes with conductive porous materials, such as porous carbon materials. With the increased electrical-double-layer (EDL) capacitance, the interfacial impedance could be decreased.[21] Although EDL-capacitive materials have been heavily developed to pursue a maximum charge storage ability for energy storage applications, their mechanical strength and conductivity were severely compromised, which is unbeneficial for the interfacial stability and robustness of bioelectronics and ionotronics. For example, porous graphene[22,23] or metal-oxide frameworks (MOFs)[24] with high EDL capacitances usually have poor mechanical properties (e.g., powder state for MOFs) and/or low conductivities (1–100 S cm^{-1}); poly(3,4-ethylenedioxythiophene):polystyrene sulfonate (PEDOT:PSS) hydrogels could possess both good EDL capacitance and good conductivity, but usually have a low mechanical strength (e.g., 0.1–2 MPa).[25–28] The intrinsic conflict among capacitance, conductivity, and mechanical properties severely limits the molecular design of electrode materials, as a large capacitance requires high porosity, which inevitably impairs the electrical conductance pathway and structural integrity. In addition, using rigid inert metals as the current collectors has been found to induce adverse immune responses at the implantation sites, due to the mechanical mismatch between the electronic materials and the organism (e.g., shear-induced inflammation and the consequent formation of a glial scar).[29]

It is worth noting that, rather than a high energy storage capability, the high fidelity of electron-ion interconversion independent of voltage and frequency is the core of bioelectronics and ionotronics, but this vital issue has not been addressed.[12] Therefore, based on our electrical model and analysis (Figure S1), the ideal electrode material for bioelectronics and ionotronics should have several key features simultaneously: a capacitive behavior (being electrically equivalent to a simple capacitor) with a high capacitance in a wide frequency range, a high electrical conductivity (alleviating the need for metal current collectors), and good mechanical properties (strong and flexible), along with high stability and good biocompatibility.

Forming EDLs with a large capacitance requires a conductive matrix with a large specific surface area, while both efficient electron transfer and high mechanical strength require a high matrix continuity with strong molecular interaction. Thus, we propose that a polymer network with interconnected nanosized pores and dense pore walls in a continuous, highly oriented arrangement would be an ideal structure for an electrode material that integrates high mechanical strength and high electrical conductivity with a capacitive behavior. Herein, we have developed a strategy, surface gelation coupled with chemical treatment and partial densification, to create conducting polymer (CP) hydrogels as exemplary model materials. Our CP hydrogels are ultrastrong (up to ~30 MPa ultimate tensile strength), highly conductive (up to

[1]Department of Materials Science and Engineering, University of California, Los Angeles, Los Angeles, CA 90095, USA

[2]School of Chemistry and Chemical Engineering, State Key Laboratory of Metal Matrix Composites, Shanghai Jiao Tong University, Shanghai 200240, China

[3]Department of Bioengineering, University of California, Los Angeles, Los Angeles, CA 90095, USA

[4]These authors contributed equally

[5]Lead contact

*Correspondence: ximinhe@ucla.edu

https://doi.org/10.1016/j.matt.2022.09.004

Please cite this article in press as: Yao et al., Ultrastrong, highly conductive and capacitive hydrogel electrode for electron-ion transduction, Matter (2022), https://doi.org/10.1016/j.matt.2022.09.004

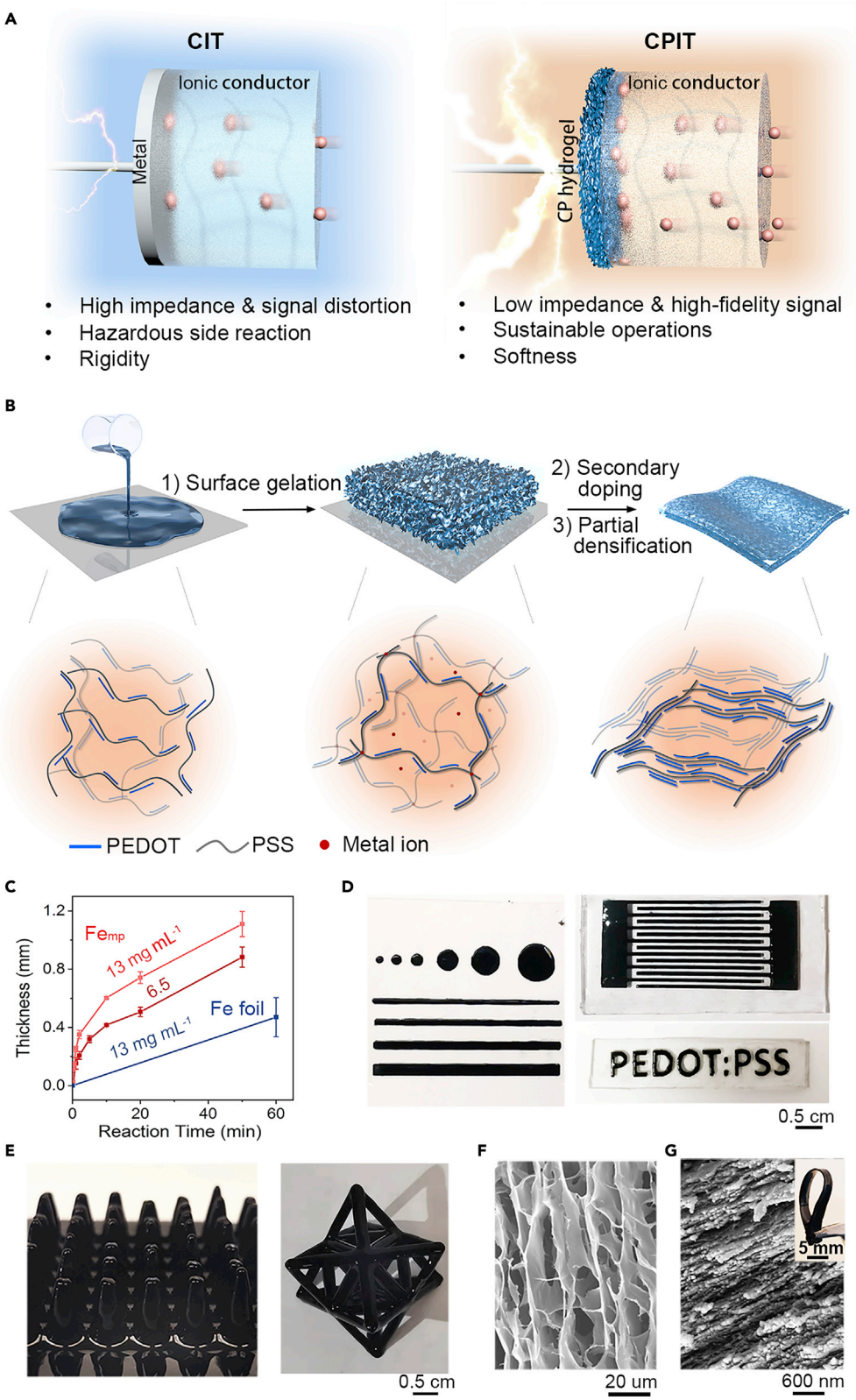

Please cite this article in press as: Yao et al., Ultrastrong, highly conductive and capacitive hydrogel electrode for electron-ion transduction, Matter (2022), https://doi.org/10.1016/j.matt.2022.09.004

Figure 1. Schematics of ionotronics and preparations of conducting polymer (CP) hydrogel

(A) Illustrative schematics of common ionotronics (CIT) with metal as the electrode and conducting-polymer-assisted ionotronics (CPIT) with PEDOT:PSS hydrogel as the electrode. Compared with CIT, CPIT has a lower interfacial impedance (electrode/electrolyte interface), a lower interfacial voltage for more sustainable operations, and a more stable signal transmission ability.

(B) Preparation procedure for CP hydrogels with the corresponding structural change of CP chains. Top: CP suspension was applied onto the surface PDMS substrate coated with Fe microparticles (Fe_{mp}) and kept static for 12 h for interfacial gelation. Then, a freestanding CP hydrogel film was obtained after chemical treatment and partial densification. The bottom illustrates the transformation of the molecular structure of CPs: the CP chains were cross-linked via electrostatic interaction between the negatively charged PSS and the Fe ions produced through *in situ* corrosion of the iron powder by the acidic PSS chains. Then, after chemical treatment and partial densification, the CP chains underwent a configurational transformation to a laminar structure with high crystallinity.

(C) Gelation kinetics of the CP suspension on the Fe_{mp}-coated PDMS or Fe foil. Before acid treatment, the thickness of the CP hydrogels prepared by dropping 13 or 6.5 mg mL^{-1} CP suspension on Fe-powder-coated PDMS substrate or Fe foil was plotted against the reaction time. Error bars represent standard deviations. See also Figure S10.

(D and E) Photographs of CP suspension selectively gelating on the patterned Fe_{mp}-coated 2D PDMS substrate (D), 3D PDMS conical pillar array (left in E), and 3D epoxy lattice structure (right in E). See also Figures S8 and S9.

(F and G) SEM images of the freeze-dried CP hydrogel before (F) and after (G) chemical treatment.

~1,200 S cm^{-1}), and capacitive (see Tables S1 and S2 for detailed comparisons), and are thus capable of serving as a freestanding electrode to convert ion-electron signals without involving metal current collectors (Figure 1A).

With these desirable properties, CP-based ionotronics (CPITs) were fabricated to demonstrate their ability to effectively solve the electron-ion transduction issues. By employing the CP hydrogel electrodes, the transduction fidelity was greatly improved, with enhanced frequency independency and voltage tolerance, through a drastic decrease in the low-frequency impedance at the electrode/ionic-conductor interfaces by nearly two orders of magnitude. Therefore, this strategy may be expected to significantly enhance the performance of various ionotronic devices, including ionic transistors, ionic-driven electric generators, and ionic-based bioelectronics. Finally, in addition to the applications in ionotronics, the benefits of CP hydrogel electrodes in bioelectronics are also demonstrated by electrical stimulation-promoted cell proliferation and excellent porcine heart pacing, with a 75% pacing voltage threshold reduction compared with commercial electrodes, further highlighting the strong ion-injection ability.

RESULTS AND DISCUSSION

Preparation of PEDOT:PSS hydrogels

The PEDOT:PSS-based CP hydrogel film was synthesized by cross-linking a commercially available CP suspension on a polydimethylsiloxane (PDMS) substrate coated with a thin layer of carbonyl Fe microparticles (Fe_{mp}) (Figures 1B, 1C, and S1–S6). The pristine PEDOT:PSS suspension is highly acidic (pH ~1.87), thus leading to the corrosion of the Fe_{mp} to form Fe^{2+} via a single displacement reaction (Table S3). In addition, part of the Fe^{2+} would be oxidized further by ambient oxygen (Figure S6). The surface gelation mechanism is mainly based on the electrostatic interaction between the PSS chains and the positively charged Fe ions, as proved by a positive shift of the zeta potential of PEDOT:PSS from −98 to −45 mV and −20 mV after the addition of 0.8 mM $FeCl_2$ and $FeCl_3$, respectively (Figure S7). Fe ions had almost no interaction with PEDOT domains as confirmed by Raman spectra and UV-vis-NIR spectra (Figure S7).

To demonstrate the attractive convenience and versatility of this surface gelation method, CP hydrogels of various 2D patterns (dot, line, bird, letters, and interdigitation) with a 150 μm resolution were fabricated on Fe_{mp}-coated PDMS simply with shadow masks (Figures 1D, S8, and S9); CP hydrogels grown on the surfaces of complex 3D structures, including lattice, curved surface, and needle array, were

Please cite this article in press as: Yao et al., Ultrastrong, highly conductive and capacitive hydrogel electrode for electron-ion transduction, Matter (2022), https://doi.org/10.1016/j.matt.2022.09.004

also constructed (Figure 1E). Moreover, bulk hydrogels with substantial thickness at the centimeter scale could also be prepared, attributable to the good diffusion of metal ions. Owing to the acidity of PSS, the fabrication could be completed by employing active metals different from Fe_{mp} as substrates (e.g., Fe, Zn, Sn, and Al foils) with all off-the-shelf chemicals (Figures S6 and S10), demonstrating the easy preparation of the CP hydrogels and potential for large-scale production. Overall, the surface gelation has a good thickness controllability and benefits conformal coating on various substrates of arbitrary geometries, 2D patterning, and 3D printability. In addition, the resulting CP network contains a large number of nanopores and restricts the excessive stacking of CP building blocks in the following chemical treatment and partial densification steps, and thus is beneficial to the EDL formation.

Yet, these as-prepared PEDOT:PSS hydrogels (CP_{ap}) with electrostatic attraction-based cross-linking are mechanically weak and possess low conductivity (<1 S cm^{-1}), not satisfying the requirements of serving as the electrodes.[30] Fortunately, their electrical and mechanical properties could be greatly improved with a chemical treatment method via phase separation and configurational transformation mechanisms. Here, H_2SO_4 was used as a treating agent due to its inexpensiveness and outstanding performance (Figures 1F and 1G).[31–33] After treatment, the metal ion cross-linker was removed by the protonation of PSS chains in the acid environment (Figure S11), while the π-π and hydrophobic interaction of PEDOT chains instead serve as nearly irreversible, strong, and dense cross-linking sites (Figures S11 and S12; Table S4). Subsequently, the pore structure, another important parameter influencing the properties of PEDOT:PSS hydrogel, was also carefully tuned by a "controlled densification" strategy, where the hydrogels were infiltrated with a diluted H_2SO_4 aqueous solution, dried, and then dialyzed in sequence. During this process, the water evaporation drove the shrinkage of micropores into nanopores and also a decrease in the hydrogel membrane thickness, while the nonvolatile H_2SO_4 prevented the full collapse of the PEDOT:PSS hydrogel to maintain the nanopores (Figure S13). The degree of such structure modifications could therefore be controlled by the water content in the H_2SO_4 solutions. Using the above method, a series of acid-treated PEDOT:PSS hydrogels with tunable mechanical and electrical properties for different practical applications was prepared, including: (1) hydrogels undergoing only the chemical treatment process with 12 or 18 M H_2SO_4 solution as treating agent (namely CP_{12M} or CP_{18M}) and (2) dense hydrogels prepared through controlled densification of CP_{18M} by employing a 20%, 10%, or 5% (v_{acid}/v_{water}) H_2SO_4 solution as densifying agent (namely $CP_{D20\%}$, $CP_{D10\%}$, and $CP_{D5\%}$).

Overall, as a result, the densified polymer network (pore wall) effectively improved the mechanical strength and conductivity, owing to the more numerous and stronger π-π interactions and the interconnection of the conductive PEDOT-rich domains, while a large number of nanopores enabled a high volumetric capacitance. In addition, the chemical treatment and densification processes were carried out sequentially, nearly irreversible, and independent of each other. For example, CP_{18M} could maintain its resistance and micro-/nanomorphology without swelling after being treated with a 20%, 10%, or 5% (v_{acid}/v_{water}) H_2SO_4 solution (Figure S14).

Mechanical and electrical properties

Taking full advantage of regulatable composition, configuration, crystallinity, and micro-/nanoporous morphology by chemical treatment and partial densification, we therefore obtained CP hydrogel films with tunable mechanical properties. They showed excellent high fractural strength, which increased with the H_2SO_4 concentration in the chemical treatment process and the densification degree of the

Please cite this article in press as: Yao et al., Ultrastrong, highly conductive and capacitive hydrogel electrode for electron-ion transduction, Matter (2022), https://doi.org/10.1016/j.matt.2022.09.004

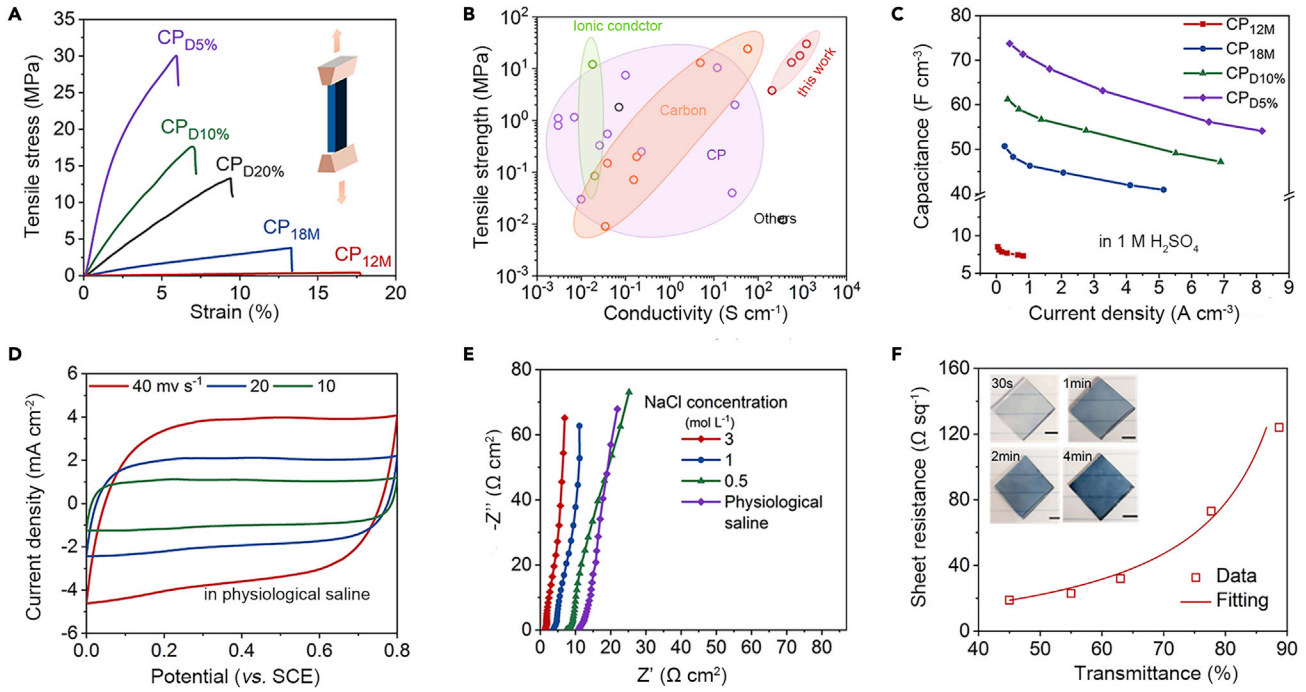

Figure 2. Properties of the PEDOT:PSS (CP) hydrogels

(A) Tensile stress-strain curves of freestanding CP hydrogels at a strain rate of 100% min^{-1}.

(B) An Ashby-style plot comparing the conductivity and strength of the CP hydrogels with the values of previously reported conductive hydrogels (including CP-based, carbon-based, and ionic-conductive hydrogels). See also Figure S15 and Table S2.

(C) Comparison of the volumetric specific capacitance of CP hydrogels in 1 M H_2SO_4 electrolyte, calculated from galvanostatic charge-discharge curves (Figures S13–S16).

(D) Cyclic voltammograms of the CP$_{18M}$ hydrogel (thickness 24 μm) at different scan rates in a three-electrode setup using physiological saline.

(E) The Nyquist plot of the CP$_{18M}$ hydrogel, tested in a three-electrode setup using physiological saline electrolyte, at a frequency range of ~10^5–0.026 Hz.

(F) Sheet-resistance vs. transmittance curve of semi-transparent CP hydrogel membrane. Insets are the optical images of a CP hydrogel membrane prepared through interfacial gelation on Fe$_{mp}$-coated PDMS substrates for different times (0.5, 1, 2, and 4 min). Scale bars, 0.5 cm. See also Figure S28.

hydrogel, much higher than those of conductive hydrogels reported previously (Figures 2A, 2B, and S15).[27,28,34] We believe this was caused by the high-degree crystallization of PEDOT chains, stronger molecular interaction, and denser laminar structure, which were verified by the morphology and structural characterizations (Figures S12 and S13).[25,33] In detail, the CP$_{D5\%}$ displayed the highest tensile strength (~30 MPa), providing outstanding structural stability for soft electronics. The CP$_{12M}$ possessed the lowest tensile strength of ~0.42 MPa with the largest fracture strain of ~17%. The conductivities of the CP hydrogels were also positively correlated with the concentrations of H_2SO_4 used in the chemical treatment process and densification degrees, increasing from 143 S cm^{-1} for CP$_{12M}$ to 1,254 S cm^{-1} for CP$_{D5\%}$, which are 10–10^3 higher than the conductivities of previously reported CP hydrogels with similar solid contents (Figure 2B).

While having these excellent mechanical properties and conductivity, the PEDOT:PSS hydrogels also showed a nearly ideal EDL capacitance, large enough for efficient electron-ion transduction when serving as both electrodes and conductors. By contrast, other porous materials explored for supercapacitors or batteries before usually suffered from either low conductance or low mechanical strength (Tables S1 and S2). For example, porous reduced graphene oxide showed a conductivity of only 30 S cm^{-1}; a conductive MOF with EDL capacitance was usually in a

Please cite this article in press as: Yao et al., Ultrastrong, highly conductive and capacitive hydrogel electrode for electron-ion transduction, Matter (2022), https://doi.org/10.1016/j.matt.2022.09.004

powder form. To compare the intrinsic electrochemical properties of CP hydrogels, a highly ionically conductive 1 M H_2SO_4 electrolyte solution was used as an electrolyte at the beginning. The cyclic voltammetry (CV) curves of all CP hydrogel films showed a quasi-rectangular shape and a linear relationship between current and scan rates ranging from 10 to 400 mV s^{-1} (Figures S16–S19), although the charge injection and/or the transport kinetics slightly limited the overall electrochemical response of electrodes as shown by weak redox peaks evolving at ~0.5 V. According to the galvanostatic charge-discharge tests (GCD) and electrochemical impedance spectra (EIS) (Figures S16–S21; Table S5), CP_{12M} showed the highest areal capacitance (128 mF cm^{-2} at 0.62 mA cm^{-2}) with the lowest volumetric capacitance (8.5 F cm^{-3} at 0.41 A cm^{-3}) among all the PEDOT:PSS hydrogels, due to the presence of micrometer pores (Figure 2C). By contrast, $CP_{D5\%}$ showed a similar areal capacitance (109 mF cm^{-2} at 0.62 mA cm^{-2}) but a significantly higher volumetric capacitance (73.7 F cm^{-3} at 0.41 A cm^{-3}) brought by its dense micromorphology. These results indicate that the majority of nanopores responsible for the EDL formation were successfully retained after the chemical treatment and densification process.

Interestingly, the CP hydrogels could still show capacitive behavior, with similar capacitances (~110 mF cm^{-2} at 0.62 mA cm^{-2}) in NaCl solutions, even physiological saline, as proved by the CV, GCD, and EIS tests (Figures 2D, 2E, and S22–S27). The good performance in the low NaCl concentrations probably was attributable to the PSS chains acting as polymer electrolytes to provide more ions for the formation of EDLs, showing attractive merit for applications in physiological environments (e.g., as bioelectronic devices for biological interface engineering).

In addition, by taking advantage of the easy processability of surface gelation, optically transparent or semi-transparent conductive PEDOT:PSS hydrogels with thicknesses of <100 nm were also fabricated by interfacial gelation reaction using a diluted CP suspension. They showed an increased sheet resistance with transmittance increase, fitting well with the theoretical equation (Figures 2F and S28). In addition, electrochemical impedance tests indicated the phase angles were near 0° within the input frequencies of 10^5–1 Hz, revealing their electronically conductive characteristics rather than ionic conductance (Figure S28).

The impedance of ionotronics

Among all the CP hydrogels developed here, $CP_{D5\%}$ has the highest conductivity (1,254 S cm^{-1}), highest mechanical strength (30 MPa), shortest fracture stain (5.9%), and highest volumetric capacitance (73.7 mF cm^{-3}), while CP_{12M} has the lowest conductivity (143 S cm^{-1}), lowest volumetric capacitance (8.5 F cm^{-3}), and highest stretchability (17%). Considering the moderate conductivity (207 S cm^{-1}), capacitance (50.7 F cm^{-3}), and mechanical properties (fracture strength 3.79 MPa, strain 13.3%), CP_{18M} hydrogels, as an example, were then selected as the model electrodes to remedy the interfacial issues of ionotronics. First, a CIT (common ionotronics, control) was fabricated by infiltrating a poly(vinyl alcohol) (PVA) hydrogel with 1 M H_2SO_4, which was then attached to two inactive metal (Pt) plates as the electrodes to connect with external circuits (inset in Figure 3A). According to the Bode impedance plots (Figure 3A), the CIT showed a low impedance of ~24 Ω with a phase angle of 0.5° at an AC voltage of 10^5 Hz, corresponding to the electrolyte resistance of the hydrogel (~20 S m^{-1}). However, upon the decrease in the alternating signal frequency, the impedance of the CIT saw a quasi-linear rise and finally reached as high as 10^4 Ω, almost 1,000 times higher than the value at 10^5 Hz. Such a high impedance at low frequencies could be mainly attributed to the high impedance of the metal/hydrogel interface.

Please cite this article in press as: Yao et al., Ultrastrong, highly conductive and capacitive hydrogel electrode for electron-ion transduction, Matter (2022), https://doi.org/10.1016/j.matt.2022.09.004

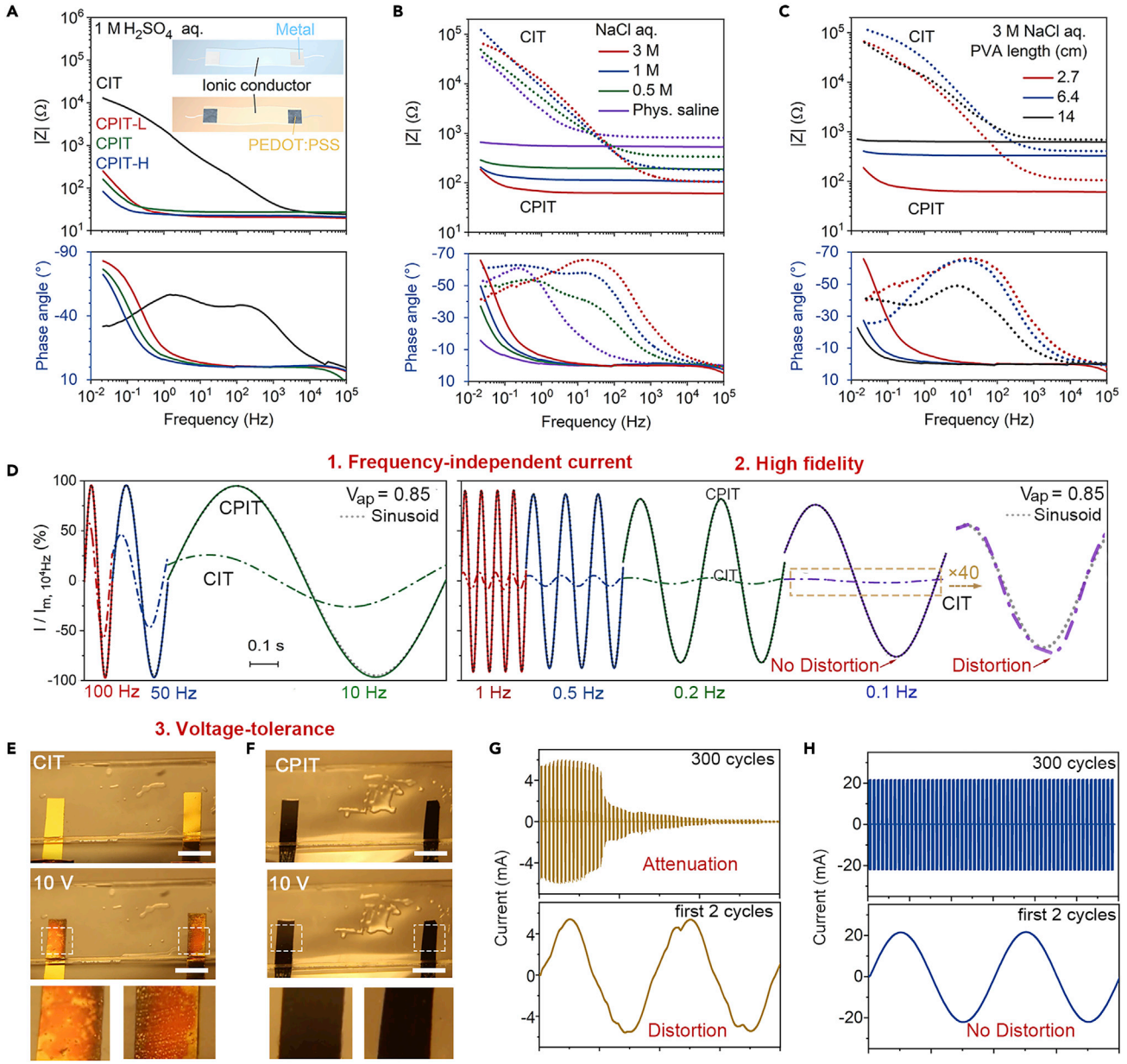

Figure 3. Electrical properties of common ionotronics (CIT) and conducting polymer-assisted ionotronics (CPIT)

(A–C) Bode plots (top, impedance; bottom, phase) of CITs and CPITs with PVA-based ionic conductors. (A) Electrodes: Pt electrode and CP_{18M} hydrogels of a high, medium, or low thickness (CPIT-H, CPIT, CPIT-L, areal capacitance 250, 120, 89 mF cm^{-2} at 0.62 mA cm^{-2}, respectively). Electrolyte: 1 M H_2SO_4 solution. Insets: schematics of CIT (top) and CPIT (bottom). (B) Electrolyte: 0.154, 0.5, 1, and 3 M NaCl solutions. Electrodes: CP_{18M} hydrogels of a medium thickness. (C) Ionic conductors: PVA hydrogels of different lengths. Electrode: CP_{18M} of a medium thickness. See also Figures S35 and S36.

(D) Normalized current vs. time curves of CITs (dashed line) and CPITs (solid line) upon sinusoidal AC voltage. For comparison, the currents were normalized to the maximum current value upon the AC voltage of 10^4 Hz. The gray dotted lines are sinusoids to clarify the deviation of the curves from the sinusoidal waveform. See also Figures S28 and S39.

(E and F) Digital photographs of CIT (E) and CPIT (F) before and after 30 cycles of sinusoidal AC voltage were applied (amplitude 10 V, frequency 1 Hz). Polyacrylamide hydrogels (16 cm × 3 cm × 1 mm) infiltrated with 1 M NaCl were used as ionic conductors. Au and $CP_{D5\%}$ were used as electrodes for CIT and CPIT, respectively. The lowest images are the enlarged dashed rectangular domains shown in the middle, indicating that the Au electrodes were corroded, while CP hydrogel electrodes remained intact. Scale bars, 1.5 cm.

(G and H) Current vs. time curves of Au-based CIT (G) and $CP_{D5\%}$-based CPIT (H) upon sinusoidal AC voltage (amplitude 10 V, frequency 1 Hz). To directly show the phase difference between current and voltage, the CIT and CPIT were shorted for 5 s (by applying a DC voltage of 0 V) right after every 5 cycles of sinusoidal AC voltage were applied. The bottom cycles are the first two cycles of the curves shown in the top. See also Figures S42, S43, and S45.

Please cite this article in press as: Yao et al., Ultrastrong, highly conductive and capacitive hydrogel electrode for electron-ion transduction, Matter (2022), https://doi.org/10.1016/j.matt.2022.09.004

Moreover, in the phase-angle vs. frequency curves (Figure 3A), upon the decrease in AC frequency from 10^3 to 0.1 Hz, the CIT showed an obvious decrease in phase angle, revealing several faradic processes initiated within the metal/hydrogel interface. These faradic processes are mainly derived from oxygen-related electrochemical reactions. For Pt electrodes, Pt-oxides and/or adsorbed oxygen atoms were formed even at a low applied voltage (offset voltage 0 V, amplitude 5 mV) (Equations 1 and 2). Although these electrochemical redox reactions are minor, their high complexity, uncontrollability, and high sensitivity to environments would severely influence the signal transduction, limiting the usages of stretchable and transparent ionotronics in terms of frequency dependence, interfacial stability, and electrical signal processing:

$$PtO_x + 2xH^+ + 2xe^- \rightleftharpoons Pt + xH_2O, \quad \text{(Equation 1)}$$

$$Pt - O_{ad} + 2H^+ + 2e^- \rightleftharpoons Pt + H_2O\,. \quad \text{(Equation 2)}$$

Alternatively, by replacing the Pt electrode with the CP_{18M} hydrogel (areal capacitance ~120 mF cm^{-2}) (Figure 3A, the green line), CPIT showed a CIT-comparable impedance of ~27 Ω at high-frequency electricity, but its impedance remained stable without significant increment upon decreasing the frequency from 10^5 to 1 Hz. In addition, the CPIT also showed a stable phase angle of ~0° within a wide frequency region, with a regular and stable increment under the low-frequency region of <1 Hz, beneficial for signal transduction and processing. The influence of the complex faradic processes on impedance, present in the CIT system, was almost negligible in the CPIT system, as the low capacitive impedance dominated the overall electrical response of the CP electrodes, although minor electrochemical redox reactions may still exist.

Our proposed CPIT strategy is a general method to ameliorate the low-frequency performance issues for different ionotronics, which was proven by using different CP hydrogels and different ionic conductors with different sizes or ionic conductivities (Figures 3B, 3C, and S29–S37; Table S6). For example, similar to the trend observed for the ionotronics with hydrogel infiltrated with H_2SO_4 as ionic conductors, all the CPITs with different NaCl electrolyte concentrations and different types or sizes of hydrogel ionic conductors showed significantly depressed impedance growth at low frequencies with stable phase angles (Figures 3B and 3C). This allows for taking full advantage of the unique properties of different hydrogels, including softness, stretchability, transparency, biocompatibility, etc., to fabricate ionotronics of high performance for different applications.

Current-time measurement, voltage response, and electrical loading

To intuitively study the conductive properties of CIT and CPIT, current-time curves were recorded when a sinusoidal AC voltage ($V(t)$) was applied ($V(t) = V_{ap}\sin(2\pi ft)$, V_{ap} is the amplitude, f is the frequency). On the whole, the evolved current showed a sinusoidal waveform with a phase difference ($\varphi_V - \varphi_I$) dependent on the EDL capacitance and ionic diffusion resistance of the ionic conductor.

At AC voltage of high frequency (10^4 Hz) and low amplitude (V_{ap}, 0.85 V), the CPIT and CIT shared a comparable current, corresponding to the electrolyte resistance of the ionic conductor, consistent with their impedance results (Figure S38). When the frequency decreased from 10^5 to 0.1 Hz, the current of the CIT saw a sharp drop to only 1% of the original value, with a phase difference of −60°, while the CPIT remained at 90% of its original current with a phase difference of −20° (Figures 3D and S39). In addition, the CIT showed an obvious deviation in the current waveform from sinusoidal shapes, especially at low-frequency AC (Figure 3D). For comparison,

the current waveforms through the CPIT were almost identical to a standard sinusoidal regardless of the input frequencies, showing the excellent advantages of the CPIT as an ionic conductor to perfectly transmit electrical signals with high quality. The high deviation in the CIT circuit could be ascribed to the significant electrochemical reaction initiated by the high voltage across the metal/electrolyte interface with a high impedance at low-frequency AC (Figure S1). The interfacial voltage (efficient voltage) can also be directly estimated by vectorially subtracting the voltage across the ionic conductor from the input voltage (Figure S39), which was calculated to be only ~0.015 V at 10 Hz and 0.038 V at 1 Hz for the CPIT at an input voltage of 0.85 V, much less than that of the CIT (~0.24 V at 10 Hz, 0.28 V at 1 Hz). In addition, the effect of the amplitude of AC power voltage was also studied. As expected, the output current increased linearly with amplitude for the CPIT with a stable phase angle, but nonlinearly for the CIT with an unstable phase angle (Figures S40 and S41), which was ascribed to the acceleration of the electrochemical reaction at the metal/electrolyte interface of the CIT at high voltages.

To visually show the high voltage tolerance of CPIT, AC voltages with high amplitudes of 1–10 V were applied (Videos S1 and S2). First, at AC voltages below 4 V, the CIT fabricated with Au electrodes (100 nm) deposited on polyester showed seriously distorted current waveforms, indicating that faradic processes strongly affected the electrical response of the electrodes (Figures S42 and S43). When the amplitude reached 10 V (Figures 3E–3H andS43), the CIT became more unstable, as shown by the current attenuation with time, accompanied by a color change of the Au electrode (from gold to red) and a gas evolution phenomenon. By contrast, when CP hydrogels ($CP_{D5\%}$) were employed as electrodes, the resultant current showed a nearly perfect sinusoidal form with a voltage-independent phase angle of 0° at a wide AC voltage range of up to 10 V (Figures 3E–3H, S44, and S45). The whole system showed high stability for at least 10,000 cycles at 10 V AC voltage, without a noticeable change in electrode appearance or gas evolution phenomenon. The good high-voltage tolerance could be attributed to the low interfacial voltage of the CP electrode, which was estimated to be only ~0.027 to 0.28 V (amplitude) at an input voltage of 1–10 V.

To have a better fundamental understanding of the electrical response of iontronics when an electrical appliance was loaded, a theoretical analysis was therefore conducted first. When loaded with a passive appliance (the equivalent circuit is shown in Figure S1), the efficient current ($|\tilde{I}|$) flowing through the circuit and the efficient interfacial voltage ($|\tilde{V}_E|$) across the hydrogel/electrode interface could be expressed by the following equations:

$$|\tilde{I}| = \frac{|\tilde{V}|}{\sqrt{(2R_0 + Z_A')^2 + \left(\frac{4}{\omega C_{EDL}} + Z_A''\right)^2}}, \quad \text{(Equation 3)}$$

$$|\tilde{V}_E| = \frac{|\tilde{V}|}{\sqrt{(\omega C_E)^2 (2R_0 + Z_A')^2 + (-4 + \omega C_E Z_A'')^2}}, \quad \text{(Equation 4)}$$

where Z_A' and Z_A'' are the real and imaginary impedances of any passive appliance loaded, R_0 and C_E represent the ionic resistance of hydrogel and capacitance of the electrode, and ω is the angular frequency of AC.

At a low-frequency signal, the induction of appliances can be neglected ($Z_A'' \leq 0$). Therefore, employing electrodes with a much higher C_E is thus expected to increase

Please cite this article in press as: Yao et al., Ultrastrong, highly conductive and capacitive hydrogel electrode for electron-ion transduction, Matter (2022), https://doi.org/10.1016/j.matt.2022.09.004

the efficient current and lower the voltage applied to the EDL, which is beneficial for the voltage tolerance and electrochemical stability of ionotronics. By mathematical approximations, when C_E increases, the current will increase linearly when the loaded appliance has a much smaller impedance than that of EDL in ionotronics ($4/\omega C_E$), or the interfacial voltage will decrease inverse to C_{EDL} when a high-impedance appliance is loaded (Figure S1).

Based on this analysis, we experimentally validated the effectiveness of a highly capacitive electrode in improving voltage tolerance and signal fidelity. A CPIT or CIT was connected to the electrical loads (20–2,000 Ω resistors as examples) with an AC power source (amplitude 0.85 V). The voltage and power of the electrical loads decreased markedly with the decrease in AC frequency for the CIT-based circuit (Figures 4A, 4B, S46, and S47), but remained excellently stable and high within a wide AC frequency range of 0.1–1,000 for the CPIT-based circuit. Then, for a more visualized demonstration, two LEDs with antiparallel polarity were also powered by an AC voltage with a triangular waveform (voltage window −3 to 3 V) (Figures 4C, S48, and S49). Overall, the voltage across the LEDs shows a nonlinear change with input voltage from 2.3 to 3 V, due to the nonlinear voltage-dependent resistance of the LED. According to the current-voltage curves (Figures 4D, 4E, and S49–S54), the CIT-based circuit showed a scan-rate-dependent curve with significant hysteresis and small current (Figure 4D), indicating the large capacitive impedance of CIT. By contrast, the CPIT-based circuit showed a simple voltage-dependent current without obvious hysteresis during the scanning cycles, showing the great convenience of LED illumination control.

Ionotronics with spatially resolved current densities

By taking advantage of the ability of the CP hydrogel to tune local interfacial impedance, a soft ionotronic model with the controlled spatial distribution of current density was demonstrated, which will be highly useful for realizing multipoint selective electrical stimulation with a simple device configuration in neuromodulation applications, for example. Here, an exemplary ionotronics model was fabricated by coating a polyacrylic acid (PAAc) hydrogel ionic conductor with patterned CP_{18M} hydrogels (Figure 4F). For measurements, the ionic conductor was divided into nine sections connected in parallel to an AC power source, and then the current through each was measured in real time. The spatial distribution of current density can be controlled by the presence (or absence) of the CP hydrogel (Figures 4G and 4H). As shown in the time-dependent current profiles, at AC power of 10 Hz, the current densities of the sections with four pieces of CP_{18M} larger current were calculated to be ∼25 mA cm^{-2}, slightly higher than those with two pieces (∼16 mA cm^{-2}). By contrast, the section without CP hydrogel showed only ∼10% of the current density of the sections with four pieces. This demonstrated that having the CP_{18M} on a hydrogel ionic conductor could effectively boost the current passing through this region, with respect to the regions not covered by CP (Figures S55 and S56; Table S7). Furthermore, when the AC power frequency decreased down to 1 Hz, the current density of the section without CP hydrogel reduced markedly by more than 50%, reaching only 5% of the current relative to that of the section with four pieces of CP hydrogel (∼21 mA cm^{-2}) (Figures 4G, 4H, and S57; Table S7). In addition, all the sections with CP_{18M} showed a sinusoidal-shaped waveform, but irregular shapes were observed for sections in the absence of CP_{18M}, as the result of severe interference of electrochemical reactions occurring within the metal/electrolyte interfaces. This ionic conductor is also stretchable (Figures 4I and S58). The CP_{18M} positions in the simulation result (the interfaces were assumed to be bonded without detachment) showed a good agreement with the experiment, indicating that the device

Please cite this article in press as: Yao et al., Ultrastrong, highly conductive and capacitive hydrogel electrode for electron-ion transduction, Matter (2022), https://doi.org/10.1016/j.matt.2022.09.004

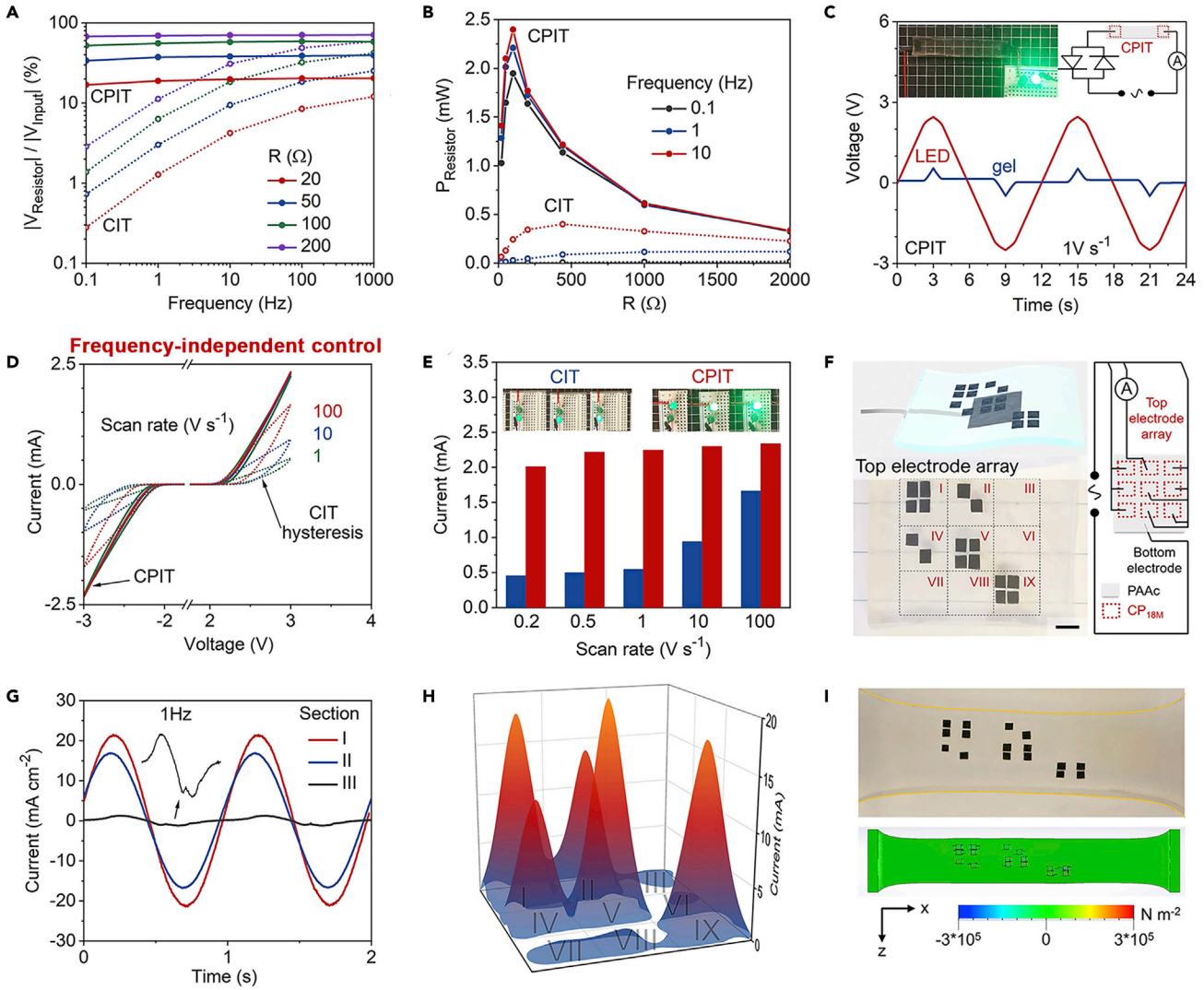

Figure 4. Demonstration of the CPIT performance and function

(A and B) Demonstration of CPITs and CITs as ionotronics connected to resistors as electrical load. (A) Voltage ratios of resistors to the peak value of input voltage ($|V_{input}|$ = 0.848 V) at different frequencies. (B) The output power of the resistors upon AC voltage of different frequencies.

(C–E) Demonstration of CPITs and CITs as ionotronics connected to LEDs as electrical loads. Two LEDs in parallel with reversed polarity were connected to an AC power source with a triangular waveform. (C) Voltage vs. time curves of the CPIT and LEDs. Voltage window, −3 to 3 V; sweep rate, 1 V s^{-1}. Insets: an optical image of the setup and the relevant circuit diagram. (D) Cyclic voltammogram of the LED circuit based on CITs (dotted lines) or CPITs (solid lines) as ionotronic devices. Scan rate, 1, 10, and 100 V s^{-1}. (E) Comparison of the current passing through LED circuits under AC voltage of different scan rates. Insets: photos of LEDs during their maximum illumination under the input voltage with different scan rates. See also Figures S48–S54.

(F–I) Demonstration of an ionotronic device with current density spatial modulation (IC-CDSM). (F) Schematic diagram (upper left) of this ionotronic device, in which several CP_{18M} hydrogels were attached to one side of an adhesive polyacrylic acid (PAAc) hydrogel as the top electrode array, while another CP_{18M} hydrogel on its opposite surface was used as the bottom electrode. The lower-left picture is a digital photograph of the top electrode. The picture on the right is a schematic diagram to depict the current measurement: the electrode array, which was divided into nine domains was connected to AC power through a Pt plate, during which the current passing through each domain was recorded by a current meter. Scale bar, 5 mm. (G and H) Electrical response of the IC-CDSM upon AC voltage (V_{eff} 0.6 V, frequency 1 Hz). (G) Current vs. time curves of domains I, II, and III on the ionotronic device. (H) Comparison of peak current densities of different domains. See also Figure S57. (I) Top: optical image of the stretched ionotronic device. The boundaries of the PAAc hydrogel are marked with yellow lines for visibility. Bottom: simulation of the shear stress along the x direction in the xz plane of the stretched IC-CDSM. Black lines indicate the boundaries of the CP_{18M} and the PAAc hydrogel.

integrity could be maintained even after stretching, owing to the excellent adhesiveness of the PAAc hydrogel. Overall, ionic conductors with spatially resolved current densities can be fabricated by patterning CP hydrogels on the surface of ionic conductors, providing an ionotronic model for multiplexed sensors and spatially resolved neural stimulators with soft, stretchable, and partially transparent properties.

Biocompatibility: Benefits in cell proliferation and heart pacing

Considering the promising applications of soft ionic-conductor-based devices in bioelectronics and the good biocompatibility of CP hydrogels as reported previously, the biological function of CP hydrogels was studied by taking advantage of their excellent conductivity. Electrical stimulations have recently been studied and employed as a strategy for therapeutic function in clinical usage, including wound healing treatment, neuron regeneration, and infarcted myocardium repair.[35] To assess the therapeutic function of our CP hydrogel, fibroblast cells, which played an essential role in the wound healing process, were incubated on our semi-transparent CP hydrogel membrane, and their behavior with electrical stimulation applied was studied *in vitro* (Figure 5A). Compared with the control group, the fibroblast cells in the group cultured with the CP hydrogel membrane with electric fields had much higher cell confluency (Figure 5B). Moreover, the LIVE/DEAD staining results showed that most of the cells were alive (green), revealing the good biocompatibility of our CP hydrogel membrane. Notably, many cells stayed round on the PEDOT:PSS hydrogel after 48 h of culturing, suggesting that our CP hydrogel membrane was nonadherent. Such a merit is vital for clinical usage to develop easily detachable devices, such as wound dressings and implantable scaffolds.[36,37] Furthermore, the cell viability and proliferation after applying electrical stimulation were measured. The cell viability reached the highest percentage after 48 h as 146.8% $\pm$ 4.27% (n = 3). The positive correlation of cell viability ratio with time represented in Figure 5C demonstrated the electric field function in facilitating fibroblast cell proliferation.

To further understand the detailed mechanism and the role of electrical stimulation through CP hydrogels in promoting cell proliferation, the growth factor expression in experimental groups was explored. The epidermal growth factor (EGF) and transforming growth factor β (TGF-β) (Figures 5D and 5E), two important growth factors involved in regulating wound healing, showed elevated expression in cells cultured on CP hydrogel upon electrical stimulation. Given the nonadhesiveness of the cells toward CP hydrogel, the enhanced expression indicates the cells should also respond to the ion flow induced by the applied AC voltage.[38,39] Upon stimulation, the Ca^{2+} ion channels of cells were opened and the intracellular Ca^{2+} concentrations changed, leading to the activation of the phosphoinositide 3-kinase/protein kinase B (PI3K/AKT) pathway for cell proliferation.[40] Therefore, the increased cell proliferation could be mapped to growth factors and cellular metabolism pathways. Owing to their powerful electron-to-ion transduction ability, CP hydrogels are therefore expected to provide an efficient approach to regulating cell proliferation, assisting wound treatment, and even potentially serving as scaffolds for promoting tissue regeneration by CP hydrogels.

Ultimately, to prove the practical applicability and advantages of the CP hydrogel in bioelectronics as a better live-tissue-electronics interface, a pair of CP electrodes with exposed areas of ~4 mm^2 was fabricated as epicardial electrodes to pace a euthanized porcine heart (Figures 5F–5H). If using commercial metal electrodes and porous Pt/C electrodes, for comparison, the pacing voltage thresholds for Au

Please cite this article in press as: Yao et al., Ultrastrong, highly conductive and capacitive hydrogel electrode for electron-ion transduction, Matter (2022), https://doi.org/10.1016/j.matt.2022.09.004

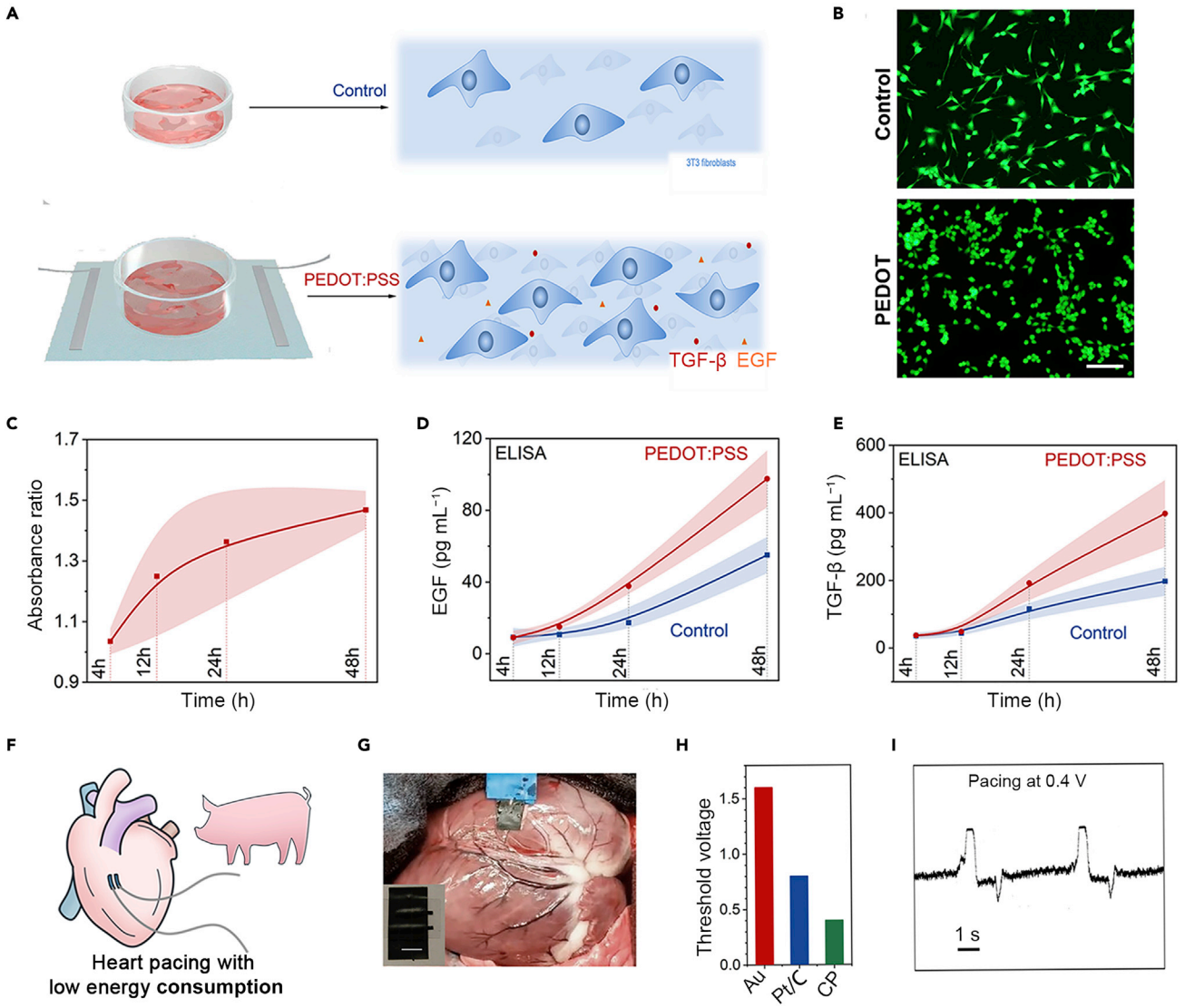

Figure 5. Biocompatibility of the CP hydrogel

(A) Schematics of fibroblasts cultured on a bare PDMS substrate (control) or a PDMS-supported CP hydrogel substrate with electrical stimulation (CP/electrical stimulation).

(B) LIVE/DEAD staining of fibroblast cells (scale bar, 100 μm). An obvious increase in cell confluency in the experimental group was observed.

(C) Absorbance ratio of cells in the CP/electrical stimulation group to those in the control group at 450 nm by Cell Counting Kit-8 (CCK-8) assay. Color bars indicate standard deviations.

(D and E) Enzyme-linked immunosorbent assay (ELISA) analysis of (D) EGF and (E) TGF-β expression concentration as a function of cell treatment time, with (red) or without (control, blue) CP/electrical stimulation. The shaded regions in (C–E) represent standard deviations calculated from three measurements.

(F–I) Demonstration of porcine heart pacing with CP hydrogel electrodes. (F and G) Illustrative schematic and photograph of CP electrodes for porcine heart pacing (scale bar, 8 mm). (H) Comparison of the threshold voltage for porcine heart pacing using different electrodes. (I) ECG signal recorded during pacing with CP hydrogel electrodes.

and Pt/C electrodes were 1.6 and 1.0 V, respectively. By contrast, the CP electrode could stimulate the heart response at a much lower voltage of 0.4 V, due to its strong electron injection ability. Such a significant stimulation power reduction of 60%–75% presents great promise for CP electrodes as a pacemaker operating with ultralow energy consumption. The successful pacing was further validated through the recording of electrocardiogram traces (Figure 5I).

Please cite this article in press as: Yao et al., Ultrastrong, highly conductive and capacitive hydrogel electrode for electron-ion transduction, Matter (2022), https://doi.org/10.1016/j.matt.2022.09.004

Conclusion and prospects

This work introduced a general strategy for preparing and utilizing ultrastrong, highly conductive, and capacitive CP hydrogel electrodes, to solve electron-ion transduction issues, including signal loss and distortion and poor voltage tolerance, which are suffered by nearly all electronics when interfacing with biological tissues or ionic conductors. Owing to the highly oriented nanoporous structures in the CP hydrogel realized by a gelation-densification strategy, these transduction issues were successfully resolved, enabling better interfacial stability and long-term operation without significant faradic electrochemical processes. Furthermore, taking advantage of the magnificent difference between CPIT and CIT, an ionic conductor with current density spatial modulation was demonstrated, providing a simple design strategy for spatially resolved ionic conductors for multiple functions of ionotronics (e.g., multipoint stimulation by a single probe). In addition, the great promotion of biological cell proliferation by electrical stimulation and significantly lower voltage threshold of heart pacing using the CP epicardial electrodes presented not only advantages in bioelectronics applications with direct tissue contact (e.g., tissue healing and neuron regenerations), but also strong ion-injection ability. This work takes a step forward for ionotronics and bioelectronics to better bridge the electronic realm with the biological world, with great promise expected in transforming human-machine interactions, energy harvesting, sensing, etc.

In addition to the hydrogel-based ionotronics, this CPIT strategy is also expected to be applicable to other subsets of ionic conductors (such as ionic liquids or polyelectrolyte-based ionotronics). The simplicity of this design, using a polymer film electrode, allows for combining other functional soft materials, such as for bio-adhesion. Moreover, considering their high conductivity, easy fabrication, and outstanding performance in reducing electrode/electrolyte interfacial impedance, CP hydrogels can be directly employed to replace metal to fabricate various ionotronics for much better performance, such as to improve the rectifying performance of ionic-based transistors, the output performance of triboelectric generators, and the signal-to-noise ratio of neural probes.

EXPERIMENTAL PROCEDURES

Resource availability

Lead contact

Further information and requests for resources should be directed to and will be fulfilled by the lead contact, Ximin He (ximinhe@ucla.edu).

Materials availability

CP hydrogels can be produced according to the procedures outlined below from commercial reagents.

Data and code availability

All experimental data are available upon request from the lead contact.

Surface gelation and patterning of CP

Typically, PDMS (Sylgard 184 silicone elastomer; Dow) plates were coated with a layer of Fe_{mp} 1–3 μm in size (40,337 iron powder, spherical; Alfa Aesar) by spray-coating a 50 mg mL^{-1} Fe_{mp} isopropanol solution (Figure S2). Subsequently, 6 mL of pristine PEDOT:PSS suspension (11–13 mg mL^{-1}, Celvios PH1000; Heraeus) was dropped onto the PDMS substrate (5.4 × 5.4 cm^2) and kept static for 12 h. Finally, CP hydrogel on PDMS was obtained after etching residual Fe_{mp} with 0.5 M

H_2SO_4. CP hydrogel with a low or high mass-loading was also prepared by using 3.5 or 8.3 mL of the pristine CP suspension as the precursor.

For patterning of the CP hydrogel, Fe_{mp}-coated PDMS was attached with a mask (Magic tape; Scotch) with a designed pattern (fabricated by a laser cutter [LS-3655; Bosslaser]). A 3 mg mL^{-1} CP suspension was dropped onto the substrate and kept still for 20 min. Finally, the CP hydrogel with patterns was obtained after removing the mask and etching the residual Fe_{mp} with 0.5 M H_2SO_4.

Preparation of the freestanding CP hydrogel

The as-prepared CP hydrogel on the PDMS substrate was chemically treated with H_2SO_4 solution with a gradient concentration from 1 to 12 mol L^{-1}. Then, the freestanding CP_{12M} was obtained after dialysis in purified water for 2 days to remove the H_2SO_4. The CP_{18M} was obtained by further treating freestanding CP_{12M} with concentrated H_2SO_4, followed by dialysis for 2 days. $CP_{D20\%}$, $CP_{D10\%}$, and $CP_{D5\%}$ were densified CP_{18M}, prepared by exchanging the water in CP_{18M} with H_2SO_4 solution of different concentrations (volumetric ratio of H_2SO_4 and water 20%, 10%, and 5%, respectively), followed by drying at 70°C for 2 h and dialysis in water for 2 days.

Preparations of optically transparent CP hydrogel membrane

A 1.5 mg mL^{-1} CP suspension was dropped onto an Fe_{mp}-coated PDMS substrate and kept static for 30 s to 5 min, followed by chemical treatment with H_2SO_4 solution with a gradient concentration from 1 to 12 mol L^{-1}. Finally, transparent CP hydrogel membranes supported by the PDMS substrate were obtained after dialysis for 12 h. The optically transparent CP hydrogels were used for the cell culture studies.

SUPPLEMENTAL INFORMATION

Supplemental information can be found online at https://doi.org/10.1016/j.matt.2022.09.004.

ACKNOWLEDGMENTS

X.H. acknowledges NSF CAREER award 1724526; AFOSR awards FA9550-17-1-0311, FA9550-18-1-0449, and FA9550-20-1-0344; and ONR awards N000141712117 and N00014-18-1-2314.

AUTHOR CONTRIBUTIONS

B.Y. and X.H. designed the research; B.Y., Y.Y., Q.C., and C.W. performed the experimental research; S.D. performed the mechanical analysis; D.W., S.W., and Y.Z. contributed reagents and analytical tools; B.Y., Y.Y., Y.D., T.H., and X.H. analyzed the data; and B.Y., Y.Y., X.Z., and X.H. wrote the paper.

DECLARATION OF INTERESTS

The authors declare no competing interests.

Received: June 3, 2022
Revised: August 29, 2022
Accepted: September 6, 2022
Published: September 23, 2022

REFERENCES

1. Yang, C., and Suo, Z. (2018). Hydrogel ionotronics. Nat. Rev. Mater. *3*, 125–142. https://doi.org/10.1038/s41578-018-0018-7.

2. Schroeder, T.B.H., Guha, A., Lamoureux, A., VanRenterghem, G., Sept, D., Shtein, M., Yang, J., and Mayer, M. (2017). An electric-eel-inspired soft power source from stacked hydrogels. Nature *552*, 214–218. https://doi.org/10.1038/nature24670.

3. Zou, Y., Tan, P., Shi, B., Ouyang, H., Jiang, D., Liu, Z., Li, H., Yu, M., Wang, C., Qu, X., et al. (2019). A bionic stretchable nanogenerator for underwater sensing and energy harvesting. Nat. Commun. *10*, 2695. https://doi.org/10.1038/s41467-019-10433-4.

4. Kim, B., Na, J., Lim, H., Kim, Y., Kim, J., and Kim, E. (2019). Robust high thermoelectric harvesting under a self-humidifying bilayer of metal organic framework and hydrogel layer. Adv. Funct. Mater. *29*, 1807549. https://doi.org/10.1002/adfm.201807549.

5. Tybrandt, K., Forchheimer, R., and Berggren, M. (2012). Logic gates based on ion transistors. Nat. Commun. *3*, 871. https://doi.org/10.1038/ncomms1869.

6. Tybrandt, K., Larsson, K.C., Richter-Dahlfors, A., and Berggren, M. (2010). Ion bipolar junction transistors. Proc. Natl. Acad. Sci. USA *107*, 9929–9932. https://doi.org/10.1073/pnas.0913911107.

7. Yang, C.H., Chen, B., Zhou, J., Chen, Y.M., and Suo, Z. (2016). Electroluminescence of giant stretchability. Adv. Mater. *28*, 4480–4484. https://doi.org/10.1002/adma.201504031.

8. Liu, X., Liu, J., Lin, S., and Zhao, X. (2020). Hydrogel machines. Mater. Today *36*, 102–124. https://doi.org/10.1016/j.mattod.2019.12.026.

9. Li, T., Li, G., Liang, Y., Cheng, T., Dai, J., Yang, X., Liu, B., Zeng, Z., Huang, Z., Luo, Y., et al. (2017). Fast-moving soft electronic fish. Sci. Adv. *3*, e1602045. https://doi.org/10.1126/sciadv.1602045.

10. Kim, D.H., Lu, N., Ghaffari, R., Kim, Y.S., Lee, S.P., Xu, L., Wu, J., Kim, R.H., Song, J., Liu, Z., et al. (2011). Materials for multifunctional balloon catheters with capabilities in cardiac electrophysiological mapping and ablation therapy. Nat. Mater. *10*, 316–323. https://doi.org/10.1038/nmat2971.

11. Wise, K.D., Anderson, D.J., Hetke, J.F., Kipke, D.R., and Najafi, K. (2004). Wireless implantable microsystems: high-density electronic interfaces to the nervous system. Proc. IEEE *92*, 76–97. https://doi.org/10.1109/jproc.2003.820544.

12. Boehler, C., Carli, S., Fadiga, L., Stieglitz, T., and Asplund, M. (2020). Tutorial: guidelines for standardized performance tests for electrodes intended for neural interfaces and bioelectronics. Nat. Protoc. *15*, 3557–3578. https://doi.org/10.1038/s41596-020-0389-2.

13. Song, E., Li, J., Won, S.M., Bai, W., and Rogers, J.A. (2020). Materials for flexible bioelectronic systems as chronic neural interfaces. Nat. Mater. *19*, 590–603. https://doi.org/10.1038/s41563-020-0679-7.

14. Zhu, B., Gong, S., and Cheng, W. (2019). Softening gold for elastronics. Chem. Soc. Rev. *48*, 1668–1711. https://doi.org/10.1039/c8cs00609a.

15. Son, D., Lee, J., Qiao, S., Ghaffari, R., Kim, J., Lee, J.E., Song, C., Kim, S.J., Lee, D.J., Jun, S.W., et al. (2014). Multifunctional wearable devices for diagnosis and therapy of movement disorders. Nat. Nanotechnol. *9*, 397–404. https://doi.org/10.1038/nnano.2014.38.

16. Chun, J., Ye, B.U., Lee, J.W., Choi, D., Kang, C.Y., Kim, S.W., Wang, Z.L., and Baik, J.M. (2016). Boosted output performance of triboelectric nanogenerator via electric double layer effect. Nat. Commun. *7*, 12985. https://doi.org/10.1038/ncomms12985.

17. Keplinger, C., Sun, J.Y., Foo, C.C., Rothemund, P., Whitesides, G.M., and Suo, Z. (2013). Stretchable, transparent, ionic conductors. Science *341*, 984–987. https://doi.org/10.1126/science.1240228.

18. Liu, J., Zhang, X., Liu, Y., Rodrigo, M., Loftus, P.D., Aparicio-Valenzuela, J., Zheng, J., Pong, T., Cyr, K.J., Babakhanian, M., et al. (2020). Intrinsically stretchable electrode array enabled in vivo electrophysiological mapping of atrial fibrillation at cellular resolution. Proc. Natl. Acad. Sci. USA *117*, 14769–14778. https://doi.org/10.1073/pnas.2000207117.

19. Yu, Y., Nyein, H.Y.Y., Gao, W., and Javey, A. (2020). Flexible electrochemical bioelectronics: the rise of in situ bioanalysis. Adv. Mater. *32*, e1902083. https://doi.org/10.1002/adma.201902083.

20. Hong, G., and Lieber, C.M. (2019). Novel electrode technologies for neural recordings. Nat. Rev. Neurosci. *20*, 330–345. https://doi.org/10.1038/s41583-019-0140-6.

21. Fang, Y., Prominski, A., Rotenberg, M.Y., Meng, L., Acarón Ledesma, H., Lv, Y., Yue, J., Schaumann, E., Jeong, J., Yamamoto, N., et al. (2021). Micelle-enabled self-assembly of porous and monolithic carbon membranes for bioelectronic interfaces. Nat. Nanotechnol. *16*, 206–213. https://doi.org/10.1038/s41565-020-00805-z.

22. Li, Z., Gadipelli, S., Li, H., Howard, C.A., Brett, D.J.L., Shearing, P.R., Guo, Z., Parkin, I.P., and Li, F. (2020). Tuning the interlayer spacing of graphene laminate films for efficient pore utilization towards compact capacitive energy storage. Nat. Energy *5*, 160–168. https://doi.org/10.1038/s41560-020-0560-6.

23. Yang, X., Cheng, C., Wang, Y., Qiu, L., and Li, D. (2013). Liquid-mediated dense integration of graphene materials for compact capacitive energy storage. Science *341*, 534–537. https://doi.org/10.1126/science.1239089.

24. Sheberla, D., Bachman, J.C., Elias, J.S., Sun, C.-J., Shao-Horn, Y., and Dincă, M. (2017). Conductive MOF electrodes for stable supercapacitors with high areal capacitance. Nat. Mater. *16*, 220–224. https://doi.org/10.1038/nmat4766.

25. Yao, B., Wang, H., Zhou, Q., Wu, M., Zhang, M., Li, C., and Shi, G. (2017). Ultrahigh-conductivity polymer hydrogels with arbitrary structures. Adv. Mater. *29*, 1700974. https://doi.org/10.1002/adma.201700974.

26. Feig, V.R., Tran, H., Lee, M., Liu, K., Huang, Z., Beker, L., Mackanic, D.G., and Bao, Z. (2019). An electrochemical gelation method for patterning conductive PEDOT:PSS hydrogels. Adv. Mater. *31*, e1902869. https://doi.org/10.1002/adma.201902869.

27. Lu, B., Yuk, H., Lin, S., Jian, N., Qu, K., Xu, J., and Zhao, X. (2019). Pure PEDOT:PSS hydrogels. Nat. Commun. *10*, 1043. https://doi.org/10.1038/s41467-019-09003-5.

28. Zhang, S., Chen, Y., Liu, H., Wang, Z., Ling, H., Wang, C., Ni, J., Çelebi-Saltik, B., Wang, X., Meng, X., et al. (2020). Room-temperature-formed PEDOT:PSS hydrogels enable injectable, soft, and healable organic bioelectronics. Adv. Mater. *32*, 1904752. https://doi.org/10.1002/adma.201904752.

29. Govindarajan, A.V., Je, M., Park, W.T., and Achyuta, A.K.H. (2012). In MEMS as implantable neuroprobes In MEMS for Biomedical Applications, S. Bhansali and A. Vasudev, eds. (Woodhead Publishing), pp. 382–386.

30. Xia, Y., and Ouyang, J. (2010). Significant conductivity enhancement of conductive poly(3, 4-ethylenedioxythiophene): poly(styrenesulfonate) films through a treatment with organic carboxylic acids and inorganic acids. ACS Appl. Mater. Interfaces *2*, 474–483. https://doi.org/10.1021/am900708x.

31. Cruz-Cruz, I., Reyes-Reyes, M., and López-Sandoval, R. (2013). Formation of polystyrene sulfonic acid surface structures on poly(3, 4-ethylenedioxythiophene): poly(styrenesulfonate) thin films and the enhancement of its conductivity by using sulfuric acid. Thin Solid Films *531*, 385–390. https://doi.org/10.1016/j.tsf.2012.12.050.

32. Kim, N., Kee, S., Lee, S.H., Lee, B.H., Kahng, Y.H., Jo, Y.R., Kim, B.J., and Lee, K. (2014). Highly conductive PEDOT: PSS nanofibrils induced by solution-processed crystallization. Adv. Mater. *26*, 2268–2272. https://doi.org/10.1002/adma.201304611.

33. Xia, Y., Sun, K., and Ouyang, J. (2012). Solution-processed metallic conducting polymer films as transparent electrode of optoelectronic devices. Adv. Mater. *24*, 2436–2440. https://doi.org/10.1002/adma.201104795.

34. Chen, G., Rastak, R., Wang, Y., Yan, H., Feig, V., Liu, Y., Jiang, Y., Chen, S., Lian, F., Molina-Lopez, F., et al. (2019). Strain- and strain-rate-invariant conductance in a stretchable and compressible 3D conducting polymer foam. Matter *1*, 205–218. https://doi.org/10.1016/j.matt.2019.03.011.

35. Nunes, S.S., Miklas, J.W., Liu, J., Aschar-Sobbi, R., Xiao, Y., Zhang, B., Jiang, J., Massé, S., Gagliardi, M., Hsieh, A., et al. (2013). Biowire: a platform for maturation of human pluripotent stem cell-derived cardiomyocytes. Nat. Methods *10*, 781–787. https://doi.org/10.1038/Nmeth.2524.

36. Hesam Mahmoudinezhad, M., Karkhaneh, A., and Jadidi, K. (2018). Effect of PEDOT:PSS in tissue engineering composite scaffold on

improvement and maintenance of endothelial cell function. J. Biosci. *43*, 307–319. https://doi.org/10.1007/s12038-018-9748-3.

37. Wang, C., Jiang, X., Kim, H.-J., Zhang, S., Zhou, X., Chen, Y., Ling, H., Xue, Y., Chen, Z., Qu, M., et al. (2022). Flexible patch with printable and antibacterial conductive hydrogel electrodes for accelerated wound healing. Biomaterials *285*, 121479. https://doi.org/10.1016/j.biomaterials.2022.121479.

38. Pinto, M.C.X., Kihara, A.H., Goulart, V.A.M., Tonelli, F.M.P., Gomes, K.N., Ulrich, H., and Resende, R.R. (2015). Calcium signaling and cell proliferation. Cell. Signal. *27*, 2139–2149. https://doi.org/10.1016/j.cellsig.2015.08.006.

39. Ferrigno, B., Bordett, R., Duraisamy, N., Moskow, J., Arul, M.R., Rudraiah, S., Nukavarapu, S.P., Vella, A.T., and Kumbar, S.G. (2020). Bioactive polymeric materials and electrical stimulation strategies for musculoskeletal tissue repair and regeneration. Bioact. Mater. *5*, 468–485. https://doi.org/10.1016/j.bioactmat.2020.03.010.

40. Zhao, M., Song, B., Pu, J., Wada, T., Reid, B., Tai, G., Wang, F., Guo, A., Walczysko, P., Gu, Y., et al. (2006). Electrical signals control wound healing through phosphatidylinositol-3-OH kinase-γ and PTEN. Nature *442*, 457–460. https://doi.org/10.1038/nature04925.